

Investigating Thermoelectric Stability under Encapsulation Using PEI-Doped CNT Films as a Model System

Fatma Abdallah, Laura Ciammaruchi, Alex Jiménez-Arguijo, El-Shazly M. Duraia, Hossam. S. Ragab, Bernhard Döring, and Mariano Campoy-Quiles*

The stability of organic semiconductors is an important topic, which in the case of organic thermoelectrics (OTEs), has not yet got the attention it deserves. This work presents a simple method which allows to characterize the stability of OTEs, using patterned ITO substrates to electrically contact encapsulated samples. The method is applied to n-doped carbon nanotube films, a well-suited reference system due to their sensitivity to changes in doping level, and used to compare the effectiveness of different encapsulation methods. In the observed films, oxygen adsorption leads to a gradual p-doping. Among the investigated barrier materials, glass performs best. Flexible alternatives like transferred films of barrier polymers also show promise, while barrier films deposited by dropcast performed worse, likely due to their inhomogeneity. Finally, Raman imaging is shown to be a useful technique to investigate degradation in OTEs.

field of application for organic materials is organic photovoltaics (OPV), which, despite achieving promising efficiencies,^[1] still struggles with the required device lifetimes.^[2,3] In addition, the methodical research of device stability first required the establishment of standardized measurement protocols.^[4,5] Organic field effect transistors (OFETs) have yet to overcome these hurdles: while OFETs performance continuously improves, long-term stability only recently came into focus.^[6] Organic thermoelectrics (OTEs), the youngest field among these, is still struggling to reach commercially viable efficiencies, yet advancing steadily. So far, little effort is expended in investigating their stability, and no standards exist yet. Long-term stability of n-type materials at elevated temperatures is of

1. Introduction

Organic materials are interesting materials for a variety of established as well as emerging electronic applications. They have already demonstrated their viability as ubiquitous light sources in organic light emitting diodes (OLEDs), and issues related to their long-term stability have been addressed to a degree sufficient as to allow for commercialization. Another promising

particular importance, since n-type materials are intrinsically unstable to oxidation in atmosphere and their efficiencies are still lagging behind those of their p-type counterparts.


The reliability of each of these technologies depends on some kind of encapsulation. As an example, for OLEDs, excellent barriers with very low water vapor transmission rates (WVTR) of well below $10^{-5} \text{ g m}^{-2} \text{ day}^{-1}$ are required, due to the high reactivity of their low work function electrodes.^[7,8] For OPV instead, the WVTR requirement is not as stringent, and is estimated at about 10^{-4} to $10^{-3} \text{ g m}^{-2} \text{ day}^{-1}$, depending on the device architecture.^[9–11] Similar values have been estimated for OFETs.^[12] OTEs are expected to be the most robust among these, mainly because of the large differences in device geometry (e.g., relatively thick films, in-plane geometry, no catastrophic failure due to pinholes), compared to OLEDs. On the other hand, thermoelectric materials are necessarily exposed to elevated temperatures, as well as to intense temperature changes.

In this work, we investigate simple ways to encapsulate thermoelectric (TE) samples of n-doped carbon nanotubes (CNTs). To that end, we present and characterize a method that allows to encapsulate and measure TE thin-film samples under controlled conditions, and which could serve to standardize TE stability measurements.

We chose CNTs, because they are a technologically relevant material, with high chemical and mechanical stabilities, and high sensitivity to doping. Compared to other organic semiconductors, for example, polymers, CNTs are a perfect test case to compare various doping and encapsulation methods, since the CNT films will not undergo any morphological changes or degradation at elevated temperatures.

F. Abdallah, Dr. L. Ciammaruchi, A. Jiménez-Arguijo, Dr. B. Döring, Dr. M. Campoy-Quiles
Materials Science Institute of Barcelona (ICMAB-CSIC)
Campus of the UAB
Bellaterra, Barcelona 08193, Spain
E-mail: mcampoy@icmab.es

F. Abdallah, Prof. H. S. Ragab
Physics Department
Faculty of Science
Arish University
El-Arish 45511, Egypt
Prof. E.-S. M. Duraia
Physics Department
Faculty of Science
Suez Canal University
Ismailia 41522, Egypt

 The ORCID identification number(s) for the author(s) of this article can be found under <https://doi.org/10.1002/admt.202000256>.

© 2020 The Authors. Published by WILEY-VCH Verlag GmbH & Co. KGaA, Weinheim. This is an open access article under the terms of the Creative Commons Attribution License, which permits use, distribution and reproduction in any medium, provided the original work is properly cited.

DOI: 10.1002/admt.202000256

In air, CNTs typically exhibit p-type properties, due to unintentional doping by adsorbed oxygen. Upon oxygen desorption, for example, by annealing in vacuum, CNTs are expected to be completely undoped with a Seebeck coefficient equal to or close to zero. Yet there are observations of n-type behavior after annealing in vacuum.^[13,14] Therefore, control of O₂ adsorption/desorption onto CNTs is a way to tune the CNT doping level, for example, by exposing the CNTs to air, or by annealing them in vacuum. Because of their 1D nature, the density of states (DOS) of CNTs exhibits van Hove singularities, which take the shape of very pronounced peaks. Because of this strongly energy-dependent (that is, non-flat) DOS, the Seebeck coefficient is very sensitive to any change in doping level.^[15]

Besides this unintentional doping by oxygen, CNTs can also be doped with a wide variety of other acceptors or donors,^[16] acting as p- and n-dopants, respectively. Still, their susceptibility to external influences, such as the aforementioned atmospheric oxygen, makes encapsulation mandatory if long-term stability is desired.

As an n-type dopant, we chose polyethylenimine (PEI), which makes a good test case due to its long history as a CNT n-type dopant.^[17–20] However, while PEI-doped CNTs were once considered to be “air-stable,”^[17,20] the scientific community has nowadays advanced considerably, and is consequently more demanding in what it considers sufficient stability.^[21]

PEI certainly is not the only viable n-type dopant. A lot of effort is put into investigating a wide variety of promising candidates, such as complexes of crown ethers and alkali salts,^[21] water-processable dye nanoparticles,^[22] polymers,^[23,24] or small molecules,^[25] to name but a few. Recent reviews on n-type CNT dopants,^[16] and n-type OTE composites,^[26] can be consulted for a more exhaustive treatment of the topic.

In this initial report, we limit ourselves to a few examples of encapsulation barrier materials. We chose glass as the “ideal” reference, as well as common barrier polymers such as ethylene vinyl alcohol (EVOH)^[27] and polyvinyl butyral (PVB) to encapsulate PEI-doped buckypapers. To quantify their stability, we monitored the changes in Seebeck coefficient and electrical conductivity over time. To simulate working conditions, samples were stored at 100 °C in the dark between measurements.

2. Results and Discussion

2.1. Thermoelectric Properties of PEI-Doped CNTs

We start our investigation with buckypapers of eDIPS CNTs, that have been n-doped with PEI, which will serve as our model system. **Figure 1a** shows the Seebeck coefficient and Raman G-peak shift of buckypapers immersed in ethanol-based solutions of PEI for increasing amounts of time. Several observations are of interest to us. First, we see that both an increased immersion time and higher concentration can be used to increase the n-doping effect. Second, after an initial rapid change, we observe saturation.

Raman spectroscopy is a well-established technique to probe any carbon system in terms of its thickness, defect density, and electronic features, just to name a few properties.^[28–32] In particular, the Raman G-peak shifts to higher/lower wavenumbers can be used to monitor and assess the doping level in

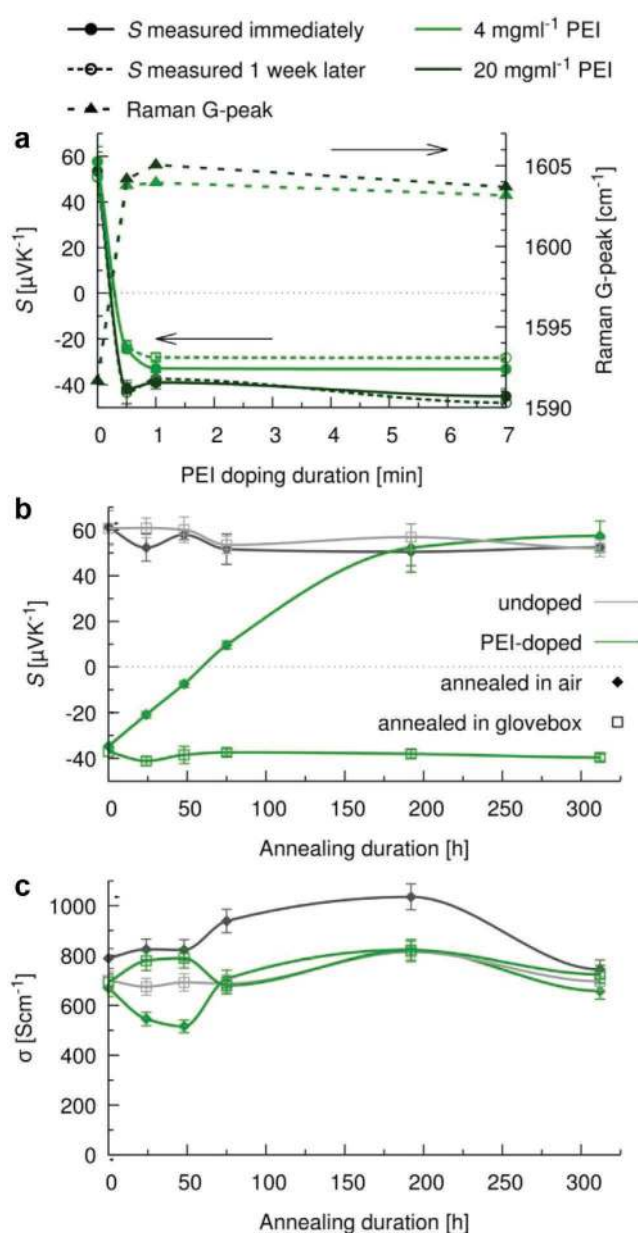


Figure 1. PEI-doped eDIPS samples. a) Effect of immersion time and PEI concentration on the Seebeck coefficient and the Raman G-peak position, both of which are correlated to the doping level. Stronger n-type doping is observed for longer immersion times, or higher concentrations of PEI in ethanol. Filled symbols are measured directly after preparation, while open symbols are remeasured after 1 week. b) Seebeck coefficient and c) electrical conductivity of undoped (gray) and PEI-doped (green) eDIPS samples annealed at 100 °C either in air, or in a N₂ glovebox. Lines are a guide to the eye.

different carbon-based materials.^[33–35] Nevertheless, it is worth to note that the specific G-peak shift being observed is the result of a (not always straightforward) combination of doping mechanism and type of nanostructured carbon (graphene, SWCNT, MWCNT, etc.). In fact, while it has been reported that charge-transfer effects may induce an up(down) G-peak shift for an electron acceptor(donor) molecule adsorption on single- and bilayer graphene,^[36] it was also shown that this effect is somehow weaker for multilayer carbon.^[37] On the other

side, chemical doping—as well as gate-induced doping—was reported to induce a G-peak up-shift for both electron and hole doping types, like boron or nitrogen.^[33,34]

In our experiment, the amine-rich polymer of PEI is believed to chemically adsorb on the CNT, as can be seen from the FTIR spectra comparison of undoped versus PEI-doped CNTs (Figure S1, Supporting Information). Compared to pristine CNT, in the amine-functionalized CNT spectrum the organic moieties of PEI clearly show up in the (2800–3000 cm^{-1}) region, together with the new absorption feature at $\approx 1440 \text{ cm}^{-1}$, corresponding to C–H stretching and bending vibrations of aliphatic hydrocarbon groups. In addition, the presence of a new strong band at $\approx 1223 \text{ cm}^{-1}$, corresponding to the C–N bond stretching, further confirms the presence of the amide functional group. Similar results for diamine-functionalized CNTs have been already reported in the literature.^[38–40]

Because the shift of the Raman G-peak is correlated to the doping level,^[28,41] it also mirrors the trend in the Seebeck coefficient (see Figures S2 and S3, Supporting information for full Raman spectra and analysis). Last, the samples are inherently unstable in air. After storing them in air in the dark for 1 week, more positive values of S are observed for the low concentration samples. For the high concentration samples, which contain more PEI, this de-doping process can take considerably longer, which is probably why PEI was initially considered to be "air-stable" in some of the early reports.^[17,20]

For further experiments, we intentionally selected an intermediate-to-low doping level of 4 mg mL^{-1} and 120 s: This way, we expect to be able to observe reasonably fast degradation of unencapsulated n-doped films.

2.2. Stability of PEI-Doped Samples

A closer look at the time-dependent Seebeck coefficient is given in Figure 1b. It reports data on both doped and undoped

samples that were annealed at $100 \text{ }^\circ\text{C}$ for extended periods, either in air or in inert atmosphere. We observe that undoped samples are stable at this temperature, independent of the surrounding atmosphere, while PEI-doped samples are only stable inside the glovebox. If exposed to oxygen, their Seebeck coefficient rapidly moves toward more positive values, until it returns to its initial value after about 200 h. The minimum in electrical conductivity coincides with the crossover from negative to positive values of the Seebeck coefficient, as is expected for an intrinsic sample, or a sample where p- and n-dopants compensate each other.

The change upon extended annealing at $100 \text{ }^\circ\text{C}$ could potentially be due to several different reasons. One possible cause could be a morphological change of the PEI upon annealing, for example, a phase separation, which is sometimes observed in the case of polymer blends. However, this would affect the samples regardless of environment, which is not what we observe. Complete decomposition of PEI is also unlikely, since it is known to be stable at this temperature.^[42]

It is more likely that the change is caused by the adsorption of oxygen, which steadily changes the level of doping. This adsorbed oxygen can either oxidize the PEI^[43,44] or reversibly physisorb onto the CNTs. To further elucidate this process, we will briefly focus on this oxygen adsorption onto neat CNTs.

2.3. Oxygen Adsorption

The effect of oxygen on the thermoelectric properties of neat eDIPS and CoMoCAT CNTs is shown in Figure 2. When CNTs are annealed in inert atmosphere, their electrical conductivity decreases, while their Seebeck coefficient increases. While S only slightly increases for eDIPS films, it triples for CoMoCAT films. The CoMoCAT tubes are rich in semiconducting tubes,

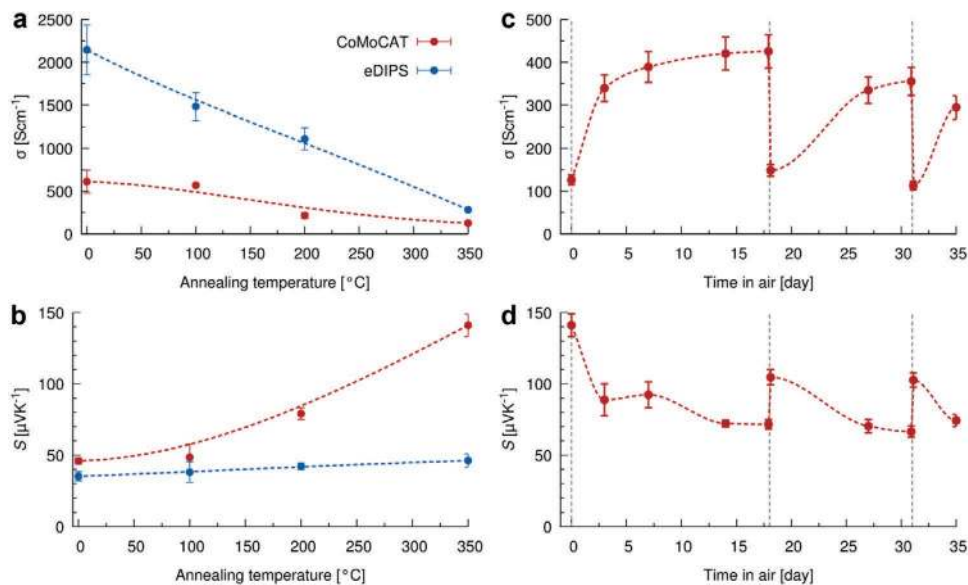


Figure 2. Effect of oxygen adsorption on CNT properties. a) Electrical conductivity and b) Seebeck coefficient of eDIPS (blue) and CoMoCAT (red) films versus annealing temperature in inert atmosphere. c) σ and d) S of unencapsulated CoMoCAT samples stored in air. Annealing samples for 1 h at $350 \text{ }^\circ\text{C}$ in inert atmosphere (indicated by the three vertical dashed lines) removes adsorbed oxygen, restoring an earlier state. The dashed lines are a guide to the eye.

and particularly in tubes with a (6,5) chiral vector. Because of the more pronounced peaks in their DOS, any change in their doping level is expected to lead to a more marked change in the TE properties. Figure 2c,d plots the evolution of a nominally undoped CoMoCAT buckypaper, that was annealed repeatedly at 350 °C for 1 h in N₂ atmosphere, and then stored and measured in air. Unlike annealing at 100 °C, which has no significant effect on neat CNTs, even after hundreds of hours (Figure 1b,c), higher annealing temperatures have a marked effect, as indicated by the vertical dashed lines. In fact, above temperatures of 300 °C, oxygen is known to desorb from the CNTs,^[13,45] which therefore changes their doping level. This is why after each annealing step, the electrical conductivity σ starts out rather low, while the Seebeck coefficient S is high. As samples are stored in air and time passes, oxygen is reabsorbed, σ increases and S decreases. When repeating the annealing, the values of S and σ can be returned close to their initial values, demonstrating a mostly reversible process. Ideally, after annealing, samples should return to the exact same values of S and σ . The deviation on the first measurement is attributed to the high sensitivity of S to small changes in doping level, particularly important for semiconductor-enriched CNT batches, as well as to the experimental limitation related to the fact that measurements are not instantaneous.

In the following, we want to use these predictable changes of S and σ of both neat and PEI-doped CNTs in the presence of oxygen, to compare different encapsulation methods to each other.

2.4. Encapsulation

In order to reliably characterize and compare different types of samples and encapsulations, we used glass substrates with patterned conductive contacts, as sketched in Figure 3a. This way, the complete sample can be enclosed, with only the conductive contacts passing through the encapsulation. Two types of conductors were used. For the initial experiment, we used silver paint, while etched ITO was used for all subsequent experiments. Importantly, the contribution of the conductor to the measured Seebeck voltage is small, since the applied temperature gradient drops across the buckypaper, and not across the conductor itself. Furthermore, any stray contributions, for example, from a slightly inhomogeneous temperature distribution across the copper heating blocks, are of the order of μV , since the Seebeck coefficient of ITO and silver is only about -12 and $2 \mu\text{V K}^{-1}$ respectively, as determined by reference measurements.

These buckypaper–conductor–glass assemblies were then encapsulated using one of several different methods described in the following sections and sketched in Figure 3.

In a first experiment, we again looked at CoMoCAT films annealed at 350 °C for 1 h inside an N₂ glovebox. After the annealing, which was performed in order to drive S to negative values, all films were encapsulated using resin and glass cover slides, and then stored at room temperature in air. Some samples were encapsulated inside the glovebox, while others were taken out and exposed to atmosphere for a few minutes before encapsulation. As can be seen from Figure 4, the

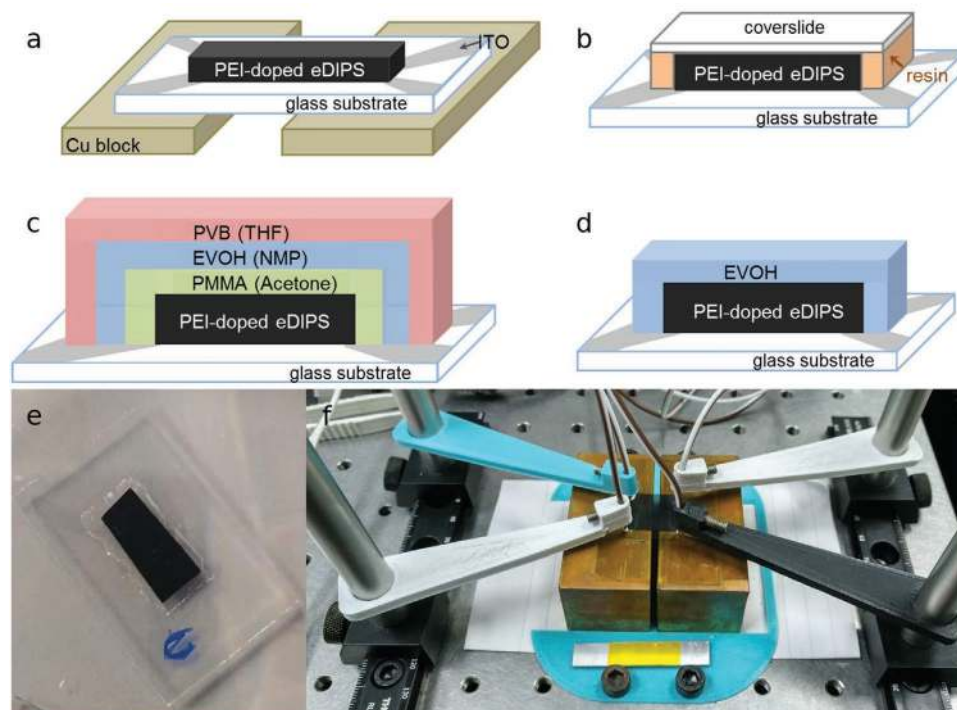


Figure 3. Sketches and photographs of samples. a) A glass substrate with a patterned conductor is used to contact the corners of a 20 by 10 mm² buckypaper sample. Copper blocks are used to heat one side of the sample, while the opposite side is maintained at room temperature. b) Sketch of the glass-encapsulated sample, c) the multilayer dropcast encapsulation, and d) the transferred EVOH sample. e) Photograph of a sample encapsulated using a multilayer dropcast, f) as well as of an unencapsulated sample mounted in the measurement setup.

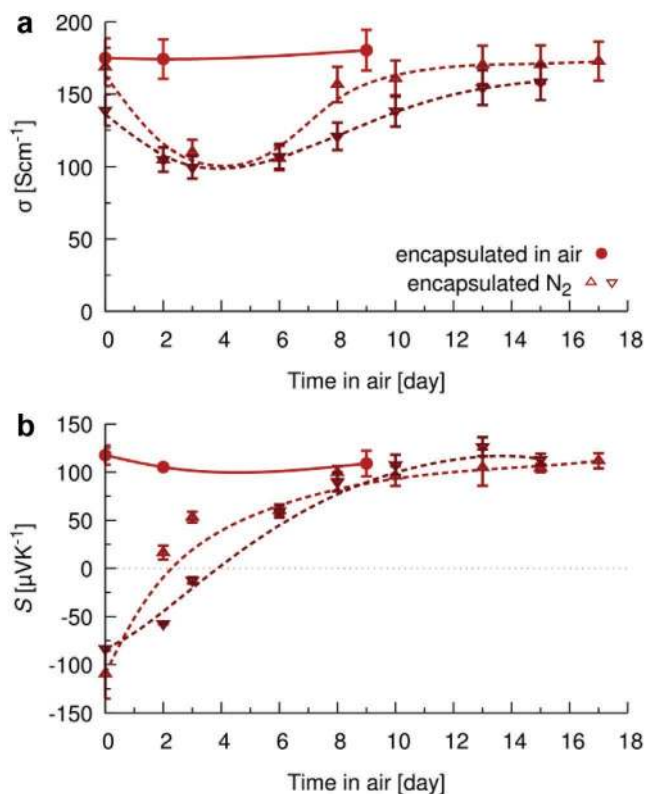


Figure 4. Thermoelectric parameters of encapsulated CoMoCAT samples stored at room temperature in air. a) Electrical conductivity and b) Seebeck coefficient of samples strongly change upon exposure to air. Two sets of samples encapsulated in N_2 are shown. The dashed lines are a guide to the eye.

unexposed samples initially exhibit $S < 0$, while the exposed samples no longer do. While we initially expected $S \approx 0$ for annealed samples without any residual oxygen, $S < 0$ is not unheard of.^[13,14] In particular, S of these almost completely dedoped samples is very sensitive to any change in the doping level,^[15,46] and air exposure has a quick and marked effect. In fact, we were not able to prepare any n-type samples by encapsulating outside of the glove box, no matter how short the exposure time was. This serves to demonstrate that even a small amount of oxygen, such as that trapped inside the encapsulated volume, is enough to return the films toward their original oxidized state. Compared to the exposed samples, which returned close to their initial, unannealed state even before the first measurement could be conducted, S of unexposed samples changes at a much slower pace. Still, the unexposed samples are not perfectly stable, because in this set of experiments, the electrical contacts were made with silver paste instead of ITO, which may compromise the encapsulation somewhat. Even so, they maintained $S < 0$ for several days. σ behaves as expected, exhibiting a minimum just as S crosses from negative to positive values, corresponding to a minimally doped system.

Although no encapsulation is perfect, we successfully slowed down degradation from a timescale of minutes to days, and validated that this method can be used to characterize encapsulated TE thin films.

After confirming that neat encapsulated CNT samples behave similarly to the ones in the glove box, we now explore different ways to encapsulate PEI-doped eDIPS films.

2.4.1. Glass and Resin

As in the previous section, encapsulation for the following experiment was realized with glass cover slides bonded to the glass substrate using UV-curable resin. Both the encapsulated and the unencapsulated samples of PEI-doped eDIPS are then continuously annealed in air at 100°C , and measured every few days. The results are shown in Figure 5a. Just as for unencapsulated samples annealed in inert atmosphere, reported in Figure 4, the encapsulated samples maintain a stable S over the investigated duration, while the exposed samples steadily degrade, crossing $S = 0$ in roughly 48 h.

It is well known that glass is a good encapsulant. Not only because it has very good gas-barrier properties,^[47] but also because it is used as a relatively thick film. But it may not be the first choice as a barrier. Other, flexible materials that are solution or roll-to-roll processable may be preferable, particularly for future applications of supposedly cheap, mass-produced organic electronics.

2.4.2. Polymer Dropcasts

In this section, we investigate whether dropcasts of one or several polymers deposited on top of the buckypapers, could serve as a simple way to encapsulate them.

One well-known barrier polymer is the copolymer poly(vinyl alcohol-co-ethylene) (EVOH), which is used commercially as an oxygen barrier.^[27] Likewise, another option is PVB, a mechanically very resistant polymer.^[48]

While EVOH is a promising encapsulant, its processing requires the use of solvents like DMSO or *N*-methyl-2-pyrrolidone (NMP), the use of which proved to be tricky. In our initial experiments, the PEI-doped buckypaper ended up being strongly affected by these solvents when a dropcast was deposited on top. This is likely related to both the solubility of PEI in these solvents, as well as to the rather high boiling point and the comparatively long time for the complete solvent evaporation. This led to a strongly reduced electrical conductivity, and in extreme cases, even to a change of the Seebeck coefficient toward more positive values.

Therefore, we opted to use a primary layer of poly(methyl methacrylate) (PMMA), deposited from acetone, to somewhat shield the doped buckypaper from being affected during subsequent depositions. Furthermore, while EVOH is an excellent oxygen barrier, its barrier properties decrease in humid environments,^[49] which we intended to counteract by depositing a top layer of PVB. Figure 5b,c shows results for four samples encapsulated with an increasing number of polymer dropcasts.

A few things can be observed. As expected, when annealed at 100°C , the unencapsulated samples degrade fastest. The encapsulated samples are more stable, and consistently able to delay degradation, even though they are far from being as stable as the glass-encapsulated sample reported in Figure 5a.

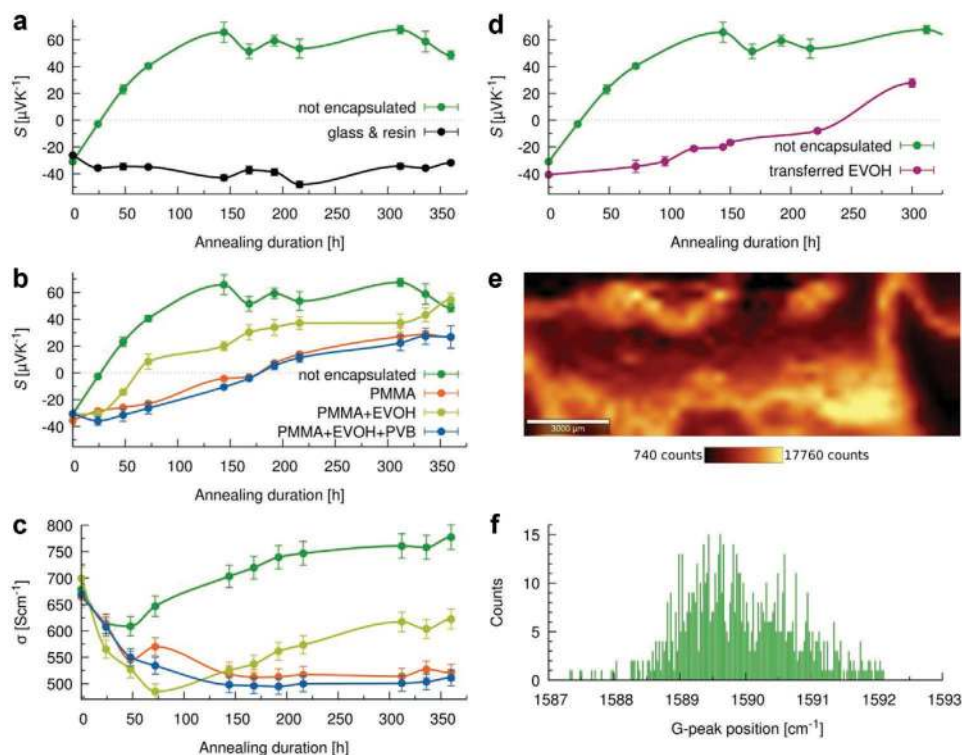


Figure 5. Evolution of TE properties of encapsulated PEI-doped eDIPS samples stored at 100 °C. a) S for films with and without encapsulation by resin and glass cover slide. b) S and c) σ for samples encapsulated by consecutive polymer dropcasts. d) S for samples encapsulated with a transferred EVOH film. e) Large-area map of the Raman signal intensity of a sample encapsulated by a triple layer of PMMA + EVOH + PVB. f) Corresponding histogram of the G-peak distribution.

As expected, the electrical conductivity of all samples decreases as the Seebeck coefficient approaches zero, before increasing again. However, while both S and σ start out nearly the same for all samples, σ of the unencapsulated ones seems to be somewhat lower than for the unencapsulated one after prolonged annealing. While part of this can be explained by the differences in oxidation level, some of it may be due to the encapsulation interacting with the buckypaper.

With only about a fourfold increase in the time taken for S to reach zero, compared to unencapsulated samples, these results are not entirely satisfactory. Interestingly, the PMMA + EVOH double layer performs worse than the single PMMA layer, while the triple layer of PMMA + EVOH + PVB performs best.

To explain this unexpected result, we investigated the samples using Raman spectroscopy. The Raman G-peak position has been used to locally infer the doping level,^[35,41,50] therefore any local fluctuations indicate a strongly varying doping level. Figure 5e,f shows a large-area Raman map and the corresponding histogram of the G-peak intensity of the triple layer-capped film. As can be seen, in a nominally identical area the G-peak intensity and position strongly fluctuate by about 4 cm^{-1} . The most likely cause for this variation, is a rather inhomogeneous encapsulation, for example, due to varying barrier thickness of the polymer dropcasts.

Figure S4, Supporting Information shows the Raman analysis relative to the large-area map presented in Figure 5e. The applied analysis routine detects automatically clusters of similar Raman spectra within an available map, and it represents

them by color. The whole scanned area can be divided in three sub-regions, according to their Raman signal intensity. Therefore, the three Raman spectra in Figure S4a, Supporting Information are averaged over the whole sub-map, which shows the same color for the ease of interpretation (Figure S4b, Supporting Information). In this map, the blue area is associated to an extremely thick region which limits the CNT Raman signal collection. The different intensities and FWHM displayed by the red and green Raman spectra G-peaks (Figure S4c, Supporting Information) can be related to an occurring p-doping process, likely due to some air exposure. From all this, we infer that the inhomogeneous spectral distribution over the scanned area, is a consequence of the inhomogeneous encapsulation resulting from the wet processing. As a further support to our claim, we register an up-shift of the average G-peak distribution after 30 days of air exposure of such samples, together with an increase of the S value (Figure S4e,f, Supporting Information).

2.4.3. Transfer of EVOH Films

To avoid any problems due to interactions between the doped CNT film and the encapsulation layer, we investigated another method, where the CNT film does not come into direct contact with strong solvents. As explained in the Experimental Section, this method involved the transfer of thin EVOH films on top of the buckypapers.

Table 1. Estimation of encapsulation quality. Average time in hours before PEI-doped samples annealed at 100 °C reached a Seebeck coefficient of $S = 0$, for the different encapsulation approaches.

Encapsulation type	Time [h] to reach $S = 0 \mu\text{V K}^{-1}$. Samples kept at 100 °C
None	24
Multilayer PMMA + EVOH + PVB dropcasts	178
Transferred EVOH film	240
Glass	>400

As shown in Figure 5d, the samples are more stable and the whole de-doping process is slightly slower compared to what we see even in the triple layer polymer dropcasts.

Table 1 summarizes the salient results. While glass performs best, we are confident, that by using the presented method, other promising approaches, like transferred multilayers can be investigated.

3. Conclusion

In summary, we presented a simple method to investigate the stability of OTEs. We used PEI-doped CNT films to compare the effectiveness of different encapsulation methods. The encapsulated samples were electrically contacted using patterned ITO substrates, which allowed us to track the Seebeck coefficient and the electrical conductivity over time, while keeping the OTE at 100 °C in order to simulate its working conditions. We identified oxygen adsorption as the main degradation pathway for the gradual p-doping of the films. In PEI-rich samples, this trend may be initially masked, due to the surplus of dopant. To delay this degradation, we investigated different barrier materials, among which glass performed best. Transferred films of EVOH could be a roll-to-roll compatible alternative, while films prepared by dropcast are not recommended, due to the uneven film thickness and coverage offered. Finally, we showed that Raman imaging can be used to evaluate doping homogeneity and thus the degradation mechanisms.

We hope that this work lays the groundwork for future studies on OTE stability. On the one hand, the method allows the investigation of barrier properties of, for example, polymer multilayers, and more importantly, their interaction with the OTE active material in realistic conditions. On the other hand, the method presents an easy way to study the stability of doped materials. For example, we expect future studies to disentangle the relation of stability to film thickness and dopant concentration. Investigations into differences in stability of semiconducting versus metallic CNTs should also prove interesting.

Last but not least, it would be ideal if future reports of thermoelectric performance would be accompanied by a stability estimation, since a material with an apparently mediocre performance may quickly outperform a less stable material.

4. Experimental Section

Materials: PEI (branched, $M_w = 800$ Da), EVOH (27 mol% ethylene), PVB, PMMA ($M_w = 15\,000$), sodium dodecylbenzenesulfonate (SDBS),

poly(sodium 4-styrenesulfonate) (PSSNa) ($M_w = 10^6$), NMP, and tetrahydrofuran (THF) were purchased from Sigma-Aldrich and used as received. CoMoCAT and eDIPS CNTs were obtained from Sigma-Aldrich and Meijo Nano Carbon, respectively.

Solution Preparation: CNTs were dispersed in deionized water using SDBS as the surfactant. For the experiments on neat CNTs, CoMoCAT CNTs were used. In all other cases, eDIPS CNTs were used. Typically, CNT concentrations of 0.2 mg mL^{-1} and 2 mg mL^{-1} of SDBS were used. The dispersions were homogenized for 15 min in a tip sonicator (Sonics Vibracell VC 505) at an amplitude of 40%, using a 3 mm tapered microtip while immersed in an ice bath. Afterward, dispersions were centrifuged (Hettich EBA 280) at 6000 rpm (≈ 2000 RCF) for 1 h.

CNT Film Preparation: CNT buckypapers were prepared by vacuum filtration. Typically, 15 mL of dispersion were filtered using a 47 mm diameter PTFE filter with $0.1 \mu\text{m}$ pore size or a cellulose nitrate filter with $0.2 \mu\text{m}$ pore size for CoMoCAT and eDIPS, respectively. Films were rinsed with copious amounts of water to remove any residual SDBS, before being dried in vacuum. Film thickness was about ≈ 500 nm for CoMoCAT and $\approx 5 \mu\text{m}$ for eDIPS films. The buckypapers were transferred to glass substrates, by wetting them with water or NMP, while evenly applying pressure and a temperature of 70 °C.

PEI Doping: PEI was dissolved in ethanol at concentrations of either 4 mg mL^{-1} or 20 mg mL^{-1} . CNT buckypapers were immersed in the dopant solution for 2 min except mentioned otherwise, before being dipped briefly in ethanol to remove any excess dopant solution. Finally, doped films were dried at 100 °C for 1 h in air or vacuum, depending on the experiment.

Encapsulation: Each glass substrate contained four patterned conductive contacts, which allowed to electrically bypass the encapsulation and contact the corners of each sample. For the initial experiments with CoMoCAT films, thin lines of silver paste were used. In all other experiments, patterned ITO was used. The CNT films deposited on these glass substrates were then encapsulated using one of the methods described below.

Glass and Resin: CNT films were encapsulated using a glass cover slide bonded to the glass substrate via an UV-curable acrylic resin (Loctite AA 350).

Polymer Dropcasts: EVOH was dissolved in NMP at 120 °C, PVB in THF at 50 °C and PMMA in acetone at room temperature. All solutions had a concentration of 30 mg mL^{-1} . 0.35 mL of solution was dropcast onto the n-doped buckypapers, then the solvent was completely evaporated on a hotplate. For multilayer polymer encapsulation, the process was repeated, giving films that were $90 \mu\text{m}$ thick on average. We observed that NMP was able to affect the thermoelectric properties of the n-doped buckypaper, because it can dissolve PEI. This is why PMMA, which dissolves in acetone, was deposited as the first layer, in order to shield the doped buckypaper from contact with stronger solvents during subsequent depositions.

Transfer of EVOH Films: Aside from using orthogonal solvents, unwanted interactions between layers can also be circumvented by lamination of thin films. To this end, solutions of 20 mg mL^{-1} of PSSNa in water were spin coated onto glass slides, to form a water-soluble sacrificial layer. Onto this, films of EVOH with an average thickness of $9.5 \mu\text{m}$ were dropcast. The EVOH films were floated off the substrate by dissolving the PSSNa in water. Then these freestanding films were transferred by bringing them in contact with the doped buckypapers. After drying, the edges of the EVOH film were affixed to the glass substrate by swabbing them with NMP.

Measurement of TE Properties: To simulate realistic working conditions between measurements, samples were stored in air, in the dark and at 100 °C. To quantify stability, electrical conductivity σ and the Seebeck coefficient S were measured in air using a custom setup. Both were measured on the same sample, using four contacts at the sample's corners. Electrical conductivity was measured using the van der Pauw method. The same four contacts were used to measure the Seebeck coefficient along the length and the diagonal of the sample.^[51] Temperature at the four contacts was measured using four type T thermocouples. Seebeck voltages were measured using the copper

leads of pairs of said thermocouples, while the temperature on one side was slowly ramped from 40 to 60 °C and back. The other side was kept close to room temperature. The average Seebeck coefficient was extracted from a straight line fit of the measured slope and corrected for the residual contribution of the ITO or silver, using reference samples. The reported error bars correspond to the standard deviation of the four Seebeck voltage measurements connecting pairs of contacts on the hot and cold sides, and give an indication of sample homogeneity. Voltages were acquired using a Keithley 2400 SourceMeter. Film thickness was measured with a profilometer (KLA Tencor P-16+) and a digital micrometer (Mitutoyo High-Accuracy Digimatic Micrometer) for CoMoCAT and eDIPS, respectively. The error bars of σ indicate its standard deviation, and are dominated by the error of the thickness measurement.

Raman Measurements: Raman characterization was realized on neat, as well as on PEI-doped eDIPS CNT films. Both encapsulated and unencapsulated samples were tested, and the G-peak shift was used as a qualitative measure of the local doping level of the material.^[41] All the measurements were acquired using a WITec alpha 300 RA+ confocal Raman setup, coupled to an Olympus objective with 10× magnification (NA 0.25). A 488 nm centered laser was employed and the light was focused either directly on the samples, or through the encapsulant. Depending on the encapsulation, the laser power was always controlled so that any photoinduced-degradation phenomenon could be avoided. In order to have reliable statistics, areas as large as (500 μm)² were sampled per measurement. All raw data were collected and analyzed using the WITec Project FIVE software.

Supporting Information

Supporting Information is available from the Wiley Online Library or from the author.

Acknowledgements

The authors would like to thank Aleksandr Perevedentsev for advice with the EVOH film transfer. The authors acknowledge financial support from the Spanish Ministry of Economy, Industry, and Competitiveness through the “Severo Ochoa” Program for Centers of Excellence in R&D (SEV-2015-0496), MAT2015-70850-P, and from the Generalitat de Catalunya through AGAUR 2018 PROD 00191; from CSIC through project 2015601032; and from the European Research Council (ERC) under grant agreement no. 648901. F.A., E.-S.M.D., and H.S.R would like to acknowledge the Ministry of Higher Education (MOHE) of Egypt, the National Bank of Egypt and Banque Misr for funding the fellowship to conduct this study.

Conflict of Interest

The authors declare no conflict of interest.

Keywords

carbon nanotubes, degradation, n-doping, organic thermoelectricity, stability

Received: March 20, 2020

Revised: April 24, 2020

Published online:

[1] Y. Cui, H. Yao, J. Zhang, T. Zhang, Y. Wang, L. Hong, K. Xian, B. Xu, S. Zhang, J. Peng, Z. Wei, F. Gao, J. Hou, *Nat. Commun.* **2019**, *10*, 2515.

- [2] S. Rafique, S. M. Abdullah, K. Sulaiman, M. Iwamoto, *Org. Electron.* **2017**, *40*, 65.
- [3] I. E. Jacobs, F. Wang, Z. I. B. Valdez, A. N. Ayala Oviedo, D. J. Bilsky, A. J. Moulé, *J. Mater. Chem. C* **2018**, *6*, 219.
- [4] M. O. Reese, S. A. Gevorgyan, M. Jørgensen, E. Bundgaard, S. R. Kurtz, D. S. Ginley, D. C. Olson, M. T. Lloyd, P. Morvillo, E. A. Katz, A. Elschner, O. Haillant, T. R. Currier, V. Shrotriya, M. Hermenau, M. Riede, K. R. Kirov, G. Trimmel, T. Rath, O. Inganäs, F. Zhang, M. Andersson, K. Tvingstedt, M. Lira-Cantu, D. Laird, C. McGuinness, S. Gowrisanker, M. Pannone, M. Xiao, J. Hauch, et al., *Sol. Energy Mater. Sol. Cells* **2011**, *95*, 1253.
- [5] M. V. Khenkin, E. A. Katz, A. Abate, G. Bardizza, J. J. Berry, C. Brabec, F. Brunetti, V. Bulović, Q. Burlingame, A. Di Carlo, R. Cheacharoen, Y.-B. Cheng, A. Colsmann, S. Cros, K. Domanski, M. Duszka, C. J. Fell, S. R. Forrest, Y. Galagan, D. Di Girolamo, M. Grätzel, A. Hagfeldt, E. von Hauff, H. Hoppe, J. Kettle, H. Köbler, M. S. Leite, S. Liu, Y.-L. Loo, J. M. Luther, et al., *Nat. Energy* **2020**, *5*, 35.
- [6] M. Nikolka, *MRS Commun.* **2019**, *10*, 98.
- [7] P. E. Burrows, G. L. Graff, M. E. Gross, P. M. Martin, M. Hall, E. Mast, C. C. Bonham, W. D. Bennett, L. A. Michalski, M. S. Weaver, J. J. Brown, D. Fogarty, L. S. Sapochak, *Proc. SPIE 4105, in Organic Light-Emitting Materials and Devices IV*, **2001**, p. 75.
- [8] E. G. Jeong, J. H. Kwon, K. S. Kang, S. Y. Jeong, K. C. Choi, *J. Inf. Disp.* **2019**, *20*, 1.
- [9] F. C. Krebs, *Stability and Degradation of Organic and Polymer Solar Cells*, John Wiley & Sons, Ltd, Chichester, UK **2012**.
- [10] S. Logothetidis, *Mater. Sci. Eng., B* **2008**, *152*, 96.
- [11] S. Cros, R. de Bettignies, S. Berson, S. Bailly, P. Maise, N. Lemaitre, S. Guillerez, *Sol. Energy Mater. Sol. Cells* **2011**, *95*, S65.
- [12] M.-C. Choi, Y. Kim, C.-S. Ha, *Prog. Polym. Sci.* **2008**, *33*, 581.
- [13] P. G. Collins, K. Bradley, M. Ishigami, A. Zettl, *Science* **2000**, *287*, 1801.
- [14] M. Yarali, J. Hao, M. Khodadadi, H. Brahmi, S. Chen, V. G. Hadjiev, Y. J. Jung, A. Mavrokefalos, *RSC Adv.* **2017**, *7*, 14078.
- [15] A. D. Avery, B. H. Zhou, J. Lee, E.-S. Lee, E. M. Miller, R. Ihly, D. Wesenberg, K. S. Mistry, S. L. Guillot, B. L. Zink, Y.-H. Kim, J. L. Blackburn, A. J. Ferguson, *Nat. Energy* **2016**, *1*, 16033.
- [16] L. Brownlie, J. Shapter, *Carbon* **2018**, *126*, 257.
- [17] M. Shim, A. Javey, N. W. S. Kam, H. Dai, *J. Am. Chem. Soc.* **2001**, *123*, 11512.
- [18] Y. Ryu, D. D. Freeman, C. Yu, *Carbon* **2011**, *49*, 4745.
- [19] D. D. Freeman, K. Choi, C. Yu, *PLoS One* **2012**, *7*, e47822.
- [20] C. Yu, A. Murali, K. Choi, Y. Ryu, *Energy Environ. Sci.* **2012**, *5*, 9481.
- [21] Y. Nonoguchi, M. Nakano, T. Murayama, H. Hagino, S. Hama, K. Miyazaki, R. Matsubara, M. Nakamura, T. Kawai, *Adv. Funct. Mater.* **2016**, *26*, 3021.
- [22] Y. Nonoguchi, A. Tani, T. Ikeda, C. Goto, N. Tanifuji, R. M. Uda, T. Kawai, *Small* **2017**, *13*, 1603420.
- [23] C.-K. Mai, B. Russ, S. L. Fronk, N. Hu, M. B. Chan-Park, J. J. Urban, R. A. Segalman, M. L. Chabinyc, G. C. Bazan, *Energy Environ. Sci.* **2015**, *8*, 2341.
- [24] B. Dörfling, J. D. Ryan, J. D. Craddock, A. Sorrentino, A. El Basaty, A. Gomez, M. Garriga, E. Pereiro, J. E. Anthony, M. C. Weisenberger, A. R. Goñi, C. Müller, M. Campoy-Quiles, *Adv. Mater.* **2016**, *28*, 2782.
- [25] Y. Nonoguchi, K. Ohashi, R. Kanazawa, K. Ashiba, K. Hata, T. Nakagawa, C. Adachi, T. Tanase, T. Kawai, *Sci. Rep.* **2013**, *3*, 3344.
- [26] J. Tang, Y. Chen, S. R. McCuskey, L. Chen, G. C. Bazan, Z. Liang, *Adv. Electron. Mater.* **2019**, *5*, 1970055.
- [27] C. Maes, W. Luyten, G. Herremans, R. Peeters, R. Carleer, M. Buntinx, *Polym. Rev.* **2018**, *58*, 209.
- [28] A. C. Ferrari, D. M. Basko, *Nat. Nanotechnol.* **2013**, *8*, 235.
- [29] A. C. Ferrari, J. Robertson, *Philos. Trans. R. Soc., A* **2004**, *362*, 2477.

- [30] J.-B. Wu, M.-L. Lin, X. Cong, H.-N. Liu, P.-H. Tan, *Chem. Soc. Rev.* **2018**, *47*, 1822.
- [31] J.-U. Lee, D. Yoon, H. Cheong, *Nano Lett.* **2012**, *12*, 4444.
- [32] D. López-Díaz, M. L. Holgado, J. L. García-Fierro, M. M. Velázquez, *J. Phys. Chem. C* **2017**, *121*, 20489.
- [33] A. Das, S. Pisana, B. Chakraborty, S. Piscanec, S. K. Saha, U. V. Waghmare, K. S. Novoselov, H. R. Krishnamurthy, A. K. Geim, A. C. Ferrari, A. K. Sood, *Nat. Nanotechnol.* **2008**, *3*, 210.
- [34] L. S. Panchakarla, K. S. Subrahmanyam, S. K. Saha, A. Govindaraj, H. R. Krishnamurthy, U. V. Waghmare, C. N. R. Rao, *Adv. Mater.* **2009**, *21*, 4726.
- [35] A. Das, A. K. Sood, A. Govindaraj, A. M. Saitta, M. Lazzeri, F. Mauri, C. N. R. Rao, *Phys. Rev. Lett.* **2007**, *99*, 136803.
- [36] R. Voggu, B. Das, C. S. Rout, C. N. R. Rao, *J. Phys.: Condens. Matter* **2008**, *20*, 472204.
- [37] K. S. Subrahmanyam, R. Voggu, A. Govindaraj, C. N. R. Rao, *Chem. Phys. Lett.* **2009**, *472*, 96.
- [38] T. Ramanathan, F. T. Fisher, R. S. Ruoff, L. C. Brinson, *Chem. Mater.* **2005**, *17*, 1290.
- [39] E. Basiuk (Golovataya-Dzhymbeeva), O. Ochoa-Olmos, F. Contreras-Torres, V. Meza-Laguna, E. Alvarez-Zauco, I. Puente-Lee, V. Basiuk, *J. Nanosci. Nanotechnol.* **2011**, *11*, 5546.
- [40] A. Mezni, N. B. Saber, A. S. A. Almalki, A. Gobouri, E. V. Basiuk, J. Rizo, V. A. Basiuk, T. Kumeria, A. Santos, D. Losic, T. Altalhi, *J. Nanosci. Nanotechnol.* **2017**, *9*, 712.
- [41] M. Bruna, A. K. Ott, M. Ijäs, D. Yoon, U. Sassi, A. C. Ferrari, *ACS Nano* **2014**, *8*, 7432.
- [42] V. V. Nedel'ko, B. L. Korsunskii, F. I. Dubovitskii, G. L. Gromova, *Polym. Sci. U.S.S.R.* **1975**, *17*, 1697.
- [43] A. Ahmadalinezhad, A. Sayari, *Phys. Chem. Chem. Phys.* **2014**, *16*, 1529.
- [44] K. Min, W. Choi, C. Kim, M. Choi, *Nat. Commun.* **2018**, *9*, 726.
- [45] C. J. An, Y. H. Kang, H. Song, Y. Jeong, S. Y. Cho, *J. Mater. Chem. A* **2017**, *5*, 15631.
- [46] K. Yanagi, S. Kanda, Y. Oshima, Y. Kitamura, H. Kawai, T. Yamamoto, T. Takenobu, Y. Nakai, Y. Maniwa, *Nano Lett.* **2014**, *14*, 6437.
- [47] S. Nagai, *J. Appl. Phys.* **2013**, *114*, 174302.
- [48] C. Carrot, A. Bendaoud, C. Pillon, in *Handbook of Thermoplastics*, CRC Press, Boca Raton, FL **2015**, pp. 89–137.
- [49] E. Kucukpinar, P. Doruker, *Polymer* **2004**, *45*, 3555.
- [50] A. M. Rao, P. C. Eklund, S. Bandow, A. Thess, R. E. Smalley, *Nature* **1997**, *388*, 257.
- [51] X. He, J. Yang, Q. Jiang, Y. Luo, D. Zhang, Z. Zhou, Y. Ren, X. Li, J. Xin, J. Hou, *Rev. Sci. Instrum.* **2016**, *87*, 124901.